Inorg. Chem. **2007**, *46*, 8801–8811

Planar versus Puckered Nets in the Polar Intermetallic Series EuGaTt (Tt = Si, Ge, Sn)

Tae-Soo You,[†] Yuri Grin,[‡] and Gordon J. Miller*[,†]

Department of Chemistry, Iowa State University, Ames, Iowa 50010, and Max-Planck-Institut für Chemische Physik fester Stoffe, Nöthnitzer Strasse 40, 01187, Dresden, Germany

Received June 6, 2007

The ternary polar intermetallic compounds EuGaTt (Tt = Si, Ge, Sn) have been synthesized and characterized experimentally, as well as theoretically. EuGaSi crystallizes in the hexagonal AlB_2-type structure (space group *P*6/*mmm*, $Z = 1$, Pearson symbol *hP*3) with randomly distributed Ga and Si atoms on the graphite-type planes: $a = 4.1687(6)$ Å, $c = 4.5543(9)$ Å. On the other hand, EuGaGe and EuGaSn adopt the hexagonal YPtAs-type structure (space group $P6_3/mmc$, $Z = 4$, Pearson symbol *hP*12): $a = 4.2646(6)$ Å and $c = 18.041(5)$ Å for EuGaGe; $a = 4.5243(5)$ Å and $c = 18.067(3)$ Å for EuGaSn. The three crystal structures contain formally $[GaTt]^{2-}$ polyanionic 3-bonded, hexagonal networks, which change from planar to puckered and exhibit a significant decrease in interlayer Ga–Ga distances as the size of Tt increases. Magnetic susceptibility measurements of this series of compounds show Curie–Weiss behavior above 86(5), 95(5), and 116(5) K with magnetic moments of 7.93, 7.97, and 7.99 μ_B for EuGaSi, EuGaGe, and EuGaSn, respectively, indicating a $4f^7$ electronic configuration (Eu^{2+}) for Eu atoms. X-ray absorption spectra (XAS) are also consistent with these magnetic properties. Electronic structure calculations supplemented by a crystal orbital Hamilton population (COHP) analysis identifies the synergy between atomic sizes, from both Eu and *Tt* atoms, and the orbital contributions from Eu toward influencing the structural features of EuGaTt. A multicentered interaction between planes of Eu atoms and the $[GaTt]^{2-}$ layers rather than through-space Ga–Ga bonding is seen in ELF distributions.

Introduction

Polar intermetallic compounds offer a growing collection of diverse structures and interesting physical properties to investigate.[1−3] These compounds consist of an electropositive metal, typically from one of the first three groups of the Periodic Table, including the rare-earth elements, combined with the more electronegative metals found around the Zintl line. As a classification of chemical compounds, such phases can be considered as a bridge between intermetallic compounds like Hume−Rothery phases or Laves phases on the one side[2] and Zintl phases on the other side.[4] Although most Zintl phases are semiconducting, many recent reports indicate that metallic behavior is common when there is substantial "cation covalency".[5,6] One such example is $EuGe_2$, which shows metallic behavior with antiferromagnetic ordering at ~50 K and divalent Eu.[7] The ten-electron $[Ge_2]^{2-}$ network forms puckered 3-connected layers stacked in an eclipsed fashion with Eu atoms sitting above/below the puckered six-membered rings. According to the Zintl−Klemm−Busmann electron-counting scheme,[4,8] the three-bonded, pyramidal environment surrounding each Ge atom is well suited for five valence electrons per Ge atom, that is, "Ge^-." A previous theoretical study showed that crystal orbitals with substantial Eu 5d orbital contributions drop below the Fermi level

* To whom correspondence should be addressed. E-mail: gmiller@iastate.edu. Fax: 515-294-0105.
[†] Iowa State University.
[‡] Max-Planck-Institut für Chemische Physik fester Stoffe.

(1) Häussermann, U.; Amerioun, S.; Eriksson, L.; Lee, C.-S.; Miller, G. J. *J. Am. Chem. Soc*. **2002**, *124*, 4371−4383.
(2) Westbrook, J. H., Fleischer, R. L., Ed. *Intermetallic Compounds: Principle and Practice*; Wiley: New York, 1995.
(3) Schäfer, H. *Annu. Rev. Mater. Sci.* **1985**, *5*, 1.
(4) Nesper, R., *Prog. Solid State Chem*. **1990**, *20*, 1.
(5) Miller, G. J.; Lee, C.-S.; Choe, W. In *Inorganic Chemistry Highlights*; Meyer, G., Naumann, D., Wesemann, L., Ed.; Wiley-VCH: Berlin, 2002.
(6) Klem, M. T.; Vaughy, J. T.; Harp, J. G.; Corbett, J. D. *Inorg. Chem*. **2001**, *40*, 7020−7026.
(7) Bobev, S.; Bauer, E. D.; Thompson, J. D.; Sarrao, J. L.; Miller, G. J.; Eck, B.; Dronskow-ski, R. *J. Solid State Chem*. **2004**, *177*, 3545−3552.
(8) Miller, G. J. In *Chemistry, Structure, and Bonding of Zintl Phases and Ions*; Kauzlarich, S. M., Ed.; VCH Publishers; New York, 1996; pp 1−59.

10.1021/ic701111e CCC: $37.00
Published on Web 09/20/2007

through Eu−Ge orbital interactions to provide the rationale for its metallic character.[7] Another example is $EuGa_2$, which adopts the orthorhombic KHg_2 structure, with a 3D, 4-connected net $[Ga_2]^{2-}$. The 8-electron network shows optimized bonding and is intrinsically metallic because of the presence of four-membered rings.[9]

As part of an investigation of $Eu(M_{1-x}M'_x)_2$ phases, where M and M′ are elements from Group 12−14, to study the interrelationships among valence electron count, magnetic order, and chemical bonding in various $[(M_{1-x}M'_x)_2]^{2-}$ networks, we have characterized the nine-electron series EuGaTt (Tt = Si, Ge, Sn). Recent studies on the series of ternary silicides AEGaSi (AE = Ca, Sr, Ba),[10] which are isoelectronic to EuGaGe, revealed that these compounds adopt the AlB_2-type structure with no preferred ordering of Ga and Si atoms in the graphite-type network.[11−15] These compounds are related to the superconducting AEAlSi (AE = Ca and Sr), which are being investigated for their similarities to superconducting MgB_2.[16] As reported herein, puckering of the graphite-type sheet occurs for the heavier tetralides Tt, and we discuss the influence of atomic size and electronic factors on the structural features of EuGaTt compounds.

Experimental Section

Synthesis and Chemical Analysis. EuGaSi, EuGaGe, and EuGaSn were synthesized from the pure elements in the molar ratio Eu/Ga/Tt (Tt = Si, Ge, Sn) = 1:1:1; Eu (Ames Laboratory, rod, 99.99%), Ga (Ames Laboratory, ingot, 99.99%), Si (Aldrich, piece, 99.999%), Ge (Alfa, piece, 99.999%) and Sn (Ames Laboratory, ingot, 99.99%). Pellets weighing 1.0 ± 0.2 g and containing stoichiometric mixtures of the corresponding elements were arc-melted under a high purity argon atmosphere on a water-cooled copper hearth and were remelted six times after turning to ensure homogeneity. During this procedure, we observed weight losses of ∼0.4−0.7 wt %; preparation of these materials in sealed Ta ampoules using either a high-frequency induction furnace or a conventional tube furnace yielded identical products, but the crystals extracted from these products were less suitable for subsequent diffraction experiments (see Supporting Information for further details about preparation methods and characterization of these products). During this series of experiments, we found that $Eu(Ga_{1-x}Si_x)_2$ showed a homogeneity range for the AlB_2-type structure. Thus, eight additional samples with different compositions ($0 \le x \le 1$) were prepared to check the range of substitution. Moreover, $Eu(Ga_{1-x}Ge_x)_2$ displays structural sensitivity depending upon the different compositions ($0 \le x \le 1$). However, we focus here just on compounds with equiatomic composition; the others will be discussed in a subsequent paper. On the basis of the powder X-ray diffraction patterns for these equiatomic products, EuGaSi and EuGaSn products showed proper crystallinities to obtain accurate lattice parameters and to pursue single-crystal X-ray diffraction investigations, whereas the EuGaGe product showed poor crystallinity. Therefore, only the EuGaGe pellet was wrapped with tantalum foil and annealed at 350 °C in an evacuated fused silica jacket for one week to improve its crystallinity. After heating, the furnace was turned off and allowed to cool down to room temperature. All three products appear to be stable to exposure to both air and moisture over several weeks. Analysis by energy-dispersive X-ray spectroscopy (EDXS) was conducted on a Hitachi S-2460N variable-pressure scanning electron microscope (SEM) with an Oxford Instruments Link Isis Model 200 X-ray analyzer. The corresponding pure elements were used as standards for intensity references.

Crystal Structure Determination. EuGaTt (Tt = Si, Ge, Sn) were characterized by both powder and single-crystal X-ray diffraction. Phase purity and lattice parameters were carried out on a Huber G670 Guinier image-plate powder diffraction camera with monochromatic Cu $K\alpha_1$ radiation ($\lambda = 1.54059$ Å). The step size was set at 0.005°, and the exposure time was 2 h. Data acquisition was controlled via the in situ program. The powder pattern of the EuGaSn compound showed a trace of Eu_2O_3 impurity. However, the lattice parameters obtained from the Rietveld refinements of the three X-ray patterns using program *Rietica*[17] were in very good agreement with the results of single-crystal X-ray diffraction.

For single-crystal X-ray diffraction experiments, several silvery plate- and needle-shaped crystals were selected from crushed samples. The crystals were checked for crystal quality by a rapid scan on a Bruker SMART Apex CCD diffractometer with Mo $K\alpha_1$ radiation ($\lambda = 0.71073$ Å), and then the best crystals were chosen for further data collection at 293(2) K. Single-crystal X-ray diffraction data of EuGaGe and EuGaSn were collected from three sets of 606 frames on a full sphere with 0.3° scans in ω and with an exposure time of 10 s per frame. Single-crystal X-ray diffraction data of EuGaSi were collected on a STOE IPDS diffractometer from two sets of 180 frames with an exposure time of 1 min for each frame. The angular range of 2θ was 4−56° for EuGaGe and EuGaSn and 4−70° for EuGaSi.

The intensities were extracted and then corrected for Lorentz and polarization effects using the *SAINT* program.[18] The program *SADABS*[18] was used for empirical absorption correction. The entire sets of reflections of the three compounds were matched with the hexagonal crystal system. After further analysis, the space group *P*6*mmm* was chosen for EuGaSi, whereas $P6_3/mmc$ was selected for EuGaGe and EuGaSn. The structures were solved by direct methods and refined on F^2 by full-matrix least-squares methods using the *SHELXTL* software package.[19] During the refinement process of EuGaGe, the Ga and Ge atoms could not be distinguished because the X-ray scattering factors for Ga and Ge atoms differ by at most 3.1%. Interatomic distances within a unit cell were also not useful to distinguish Ga and Ge atoms because of their similar covalent radii: r(Ga) = 1.25 Å and r(Ge) = 1.22 Å.[20] However, electronic structure calculations performed on several structural

(9) Nuspl, G.; Polborn, K.; Evers, J.; Landrum, G. A.; Hoffmann, R. *Inorg. Chem.* **1996**, *35*, 6922−6932.
(10) Meng, R. L.; Lorenz, B.; Wang, Y. S.; Cmaidalka, J.; Sun, Y. Y.; Xue, Y. Y.; Meen, J. K.; Chu, C. W. *Physica C* **2002**, *382*, 113−116.
(11) Imai, M.; Abe, E.; Ye, J.; Nishida, K.; Kimura, T.; Honma, K.; Abe, H,; Kitazawa, H. *Phys. Rev. Lett.* **2001**, *87*, 077003.
(12) Imai, M.; Nishida, K.; Kimura, T.; Abe, H. *Appl. Phys. Lett.* **2002**, *80*, 1019−1021.
(13) Imai, M.; Nishida, K.; Kimura, T.; Abe, H. *Physica C* **2002**, *377*, 96−100.
(14) Imai, M.; Nishida, K.; Kimura, T.; Kitazawa, H.; Abe, H.; Kito, H.; Yoshii, K. *Physica C* **2002**, *382*, 361−366.
(15) Lorenz, B.; Lenzi, J.; Cmaidalka, J.; Meng, R. L.; Sun, Y. Y; Xue, Y. Y.; Chu, C. W. *Physica C* **2002**, *383*, 191−196.
(16) Nagamatsu. J.; Nakagawa, N.; Muranaka, T.; Zenitani, Y.; Akimitsu, J. *Nature* **2001**, *410*, 63−64.
(17) Hunter, B. A.; Howard, C. J. *Rietica*; Australian Nuclear Science and Technology Organization: Menai, Australia, 2000.
(18) *XRD Single Crystal Software*; Bruker Analytical X-ray System: Madison, WI, 2002.
(19) *SHELXTL*, version 5.1; Bruker AXS Inc.: Madison, WI, 1998.
(20) Emsley, J. *The Elements*; Clarendon Press: Oxford, U.K., 1998.

models with different possible Ga and Ge atomic positions indicate that the atomic coordinates reported in Table 2 create the most energetically favorable structure. Details of those calculations are discussed in a subsequent section. In addition, evaluation of the corresponding displacement parameters indicates preference for the distribution seen in EuGaSn (see the Discussion section below). The chemical composition obtained from EDXS analysis, $Eu_{1.00(1)}Ga_{1.01(2)}Ge_{0.99(3)}$, very well matched the loading composition.

X-ray Absorption Spectroscopy (XAS). XAS measurements on the Eu L_{III} edge were conducted at the EXAFS beam-line A1 of HASYLAB at DESY (Hamburg, Germany). Samples were ground together with dry B_4C powder before the measurements. Wavelength selection was realized by means of a double-crystal Si(111) monochromator of four crystal modes with digitally stabilized components. The resolution was about 2 eV (fwhm) at the Eu L_{III} edge of 6977 eV. Eu_2O_3 was used as a reference during the measurement.

Magnetic Susceptibility Measurement. Temperature-dependent magnetic susceptibility measurements were conducted using a Quantum Design, MPMS-5 SQUID magnetometer. The measured temperature range was 1.8−300 K with a magnetic field range of 0.1−5.5 T. Magnetic measurements were carried out on bulk samples (approximately 300 mg) from the same preparations as the one used for powder diffraction experiments.

Computational Details. Tight-binding, linear muffin-tin orbital (TB-LMTO) calculations[21] were carried out in the atomic sphere approximation (ASA) using the Stuttgart program.[28] Exchange and correlation were treated by the local spin density approximation (LSDA).[22] All relativistic effects except spin−orbit coupling were taken into account by using a scalar relativistic approximation.[23]

In the ASA method, space is filled with overlapping Wigner−Seitz (WS) atomic spheres. The symmetry of the potential is considered spherical inside each WS sphere, and a combined correction is used to take into account the overlapping part.[24] The radii of WS spheres were obtained by requiring that the overlapping potential be the best possible approximation to the full potential, and were determined by an automatic procedure.[24] This overlap should not be too large because the error in kinetic energy introduced by the combined correction is proportional to the fourth power of the relative sphere overlap. No empty spheres (ES)[21] were used, but the overlapping maximum was adjusted to fill up the interstitial space in the unit cell of EuGaGe and EuGaSn. The WS radii are as follows: for EuGaSi, Eu = 2.22 Å, Ga = 1.35 Å, and Si = 1.44 Å; for EuGaGe, Eu1 = 2.24 Å, Eu2 = 2.14 Å, Ga = 1.45 Å, and Ge = 1.49 Å; for EuGaSn, Eu1 = 2.11 Å, Eu2 = 2.09 Å, Ga = 1.62 Å, and Sn = 1.77 Å. The basis sets included 6s, 6p, and 5d orbitals for Eu; 4s, 4p, and 4d orbitals for Ga; 3s, 3p, and 3d orbitals for Si; 4s, 4p, and 4d orbitals for Ge; 5s, 5p, and 5d orbitals for Sn. The Eu 6p, Ga 4d, Si 3d, Ge 4d, and Sn 5d orbitals were treated by the Löwdin downfolding technique,[21−23] and the Eu 4f wavefunctions were treated as core functions occupied by 7 electrons. The crystal orbital Hamilton population (COHP) curves[25] and the integrated COHP values (ICOHPs) were calculated to determine the relative influences of various interatomic orbital interactions. For the computation of electronic densities of states (DOS), band structures, and COHP curves, the 4f electrons of Eu were treated as core electrons. The *k*-space integrations were performed by the tetrahedron method.[26] The self-consistent charge density was obtained using 210 irreducible *k*-points in the Brillouin zone for the hexagonal cell. The contribution of the nonspherical part of the charge density to the potential was neglected. The spin-polarized calculations have been performed on each structure.

The electron localization function[27a] (ELF, η) was evaluated within the TB-LMTO-ASA program package[28] with an ELF module already implemented. To better understand features of chemical bonding in these phases, a topological analysis of ELF was conducted with the program *Basin*.[29] The integrated electron density in each basin, which is defined by the surface of zero flux in the ELF gradient, analogous to the procedure proposed by Bader for the electron density,[30] provides the basic information of electron counts for each basin, and additionally describes the bonding situation. The software *Amira*[31] was used to visualize ELF distributions.

Results and Discussion

Structures. EuGaTt (Tt = Si, Ge, Sn) crystallize in two different types of structure correlating to the different atomic sizes of Tt: (1) the AlB_2-type structure for EuGaSi and (2) the YPtAs-type structure for EuGaGe and EuGaSn. Important crystallographic data, atomic positions, selected interatomic distances, and thermal displacement parameters for EuGaSi, EuGaGe, and EuGaSn are listed in Tables 1−3.

EuGaSi. EuGaSi adopts a ternary version of the hexagonal AlB_2-type structure with a honeycomb-like $^2_\infty$[GaSi] planar layer as shown in Figure 1; the separation between adjacent planes is 4.5543(9) Å. During this investigation, we observed that EuGaSi is one example of a homogeneity range, $Eu(Ga_{1-x}Si_x)_2$ with $x = 0.165-0.862$, adopting the AlB_2-type structure.[32] Ga and Si atoms randomly occupy the 2d site in the unit cell. Therefore, many different local environments at each atomic site are possible. If Ga−Si interactions are preferred over Ga−Ga and Si−Si interactions, then we would expect to observe a superstructure with a *c*-axis length twice the observed value[33] and space group $P6_3/mmc$ as in ZrBeSi.[34] However, we find no additional X-ray reflections to suggest a doubling of the *c*-axis. For the possibility of in-plane ordering, the unit cell can be refined in the space group $P\bar{6}m2$,[34] which is the highest *translationengleiche* subgroup of *P*6*mmm* in which the 2d site of *P*6*mmm* splits into two distinct sites, 1d and 1f. However, for EuGaSi in $P\bar{6}m2$, each site was refined as the same 50:50 mixture of

(21) Anderson, O. K. *Phys. Rev. B* **1986**, *34*, 2439.
(22) Anderson, O. K.; Jepsen, O. *Phys. Rev. Lett.* **1984**, *53*, 2571−2574.
(23) Andersen, O. K.; Jepsen, O.; Glötzel, D. In *Highlights of Condensed Matter Theory*; Bassani, F.; Fumi, F., Tosi, M., Eds.;North-Holland: New York, 1985.
(24) Jepsen, O.; Anderson, O. K. *Z. Phys. B* **1995**, *97*, 35.
(25) Dronskowski, R.; Blochl, P. *J. Phys. Chem.* **1993**, *97*, 8617−8624.
(26) Blöchl, P. E.; Jepsen, O.; Anderson, O. K. *Phys. Rev. B* **1994**, *49*, 16223−16233.
(27) (a) Savin, A.; Flad, H. J.; Preuss, H.; von Schnering, H. G. *Angew. Chem.* **1992**, *104*, 185; *Angew. Chem., Int. Ed. Engl.* **1992**, *31*, 185. (b) Kohout, M. *Int. J. Quantum Chem.* **2004**, *97*, 651. (c) Kohout, M.; Wagner, F. R.; Grin, Yu. *Theor. Chem. Acc.* **2002**, *108*, 150. (d) Gatti, C. *Z. Kristallogr.* **2005**, *220*, 399.
(28) Jepsen, O.; Burkhardt, A.; Andersen, O. K. *The TB-LMTO-ASA Program*, version 4.7; Max-Planck-Institut für Festkörperforschung: Stuttgart, Germany, 1999.
(29) Kohout, M. *BASIN*, version 2.3; Max-Planck-Institut für Chemische Physik fester Stoffe: Dresden, Germany, 2001.
(30) Bader, R. F. W. *Atoms in Molecules: A Quantum Theory*; Oxford University Press: Oxford, U.K., 1999.
(31) *Amira visualization software*; Konrad-Zuse-Zentrum für Informationstechnik Berlin (ZIB): Berlin, Germany, 2003.
(32) You, T.-S.; Miller, G. J. Unpublished work.
(33) Wenski, G.; Mewis, A. *Z. Anorg. Allg. Chem.* **1986**, *535*, 110−122.
(34) Nielsen, J. W.; Baenziger, N. C. *Acta Crystallogr.* **1954**, *7*, 132−133.

Table 1. Crystallographic Data for EuGaTt (Tt = Si, Ge, Sn)

	EuGaSi	EuGaGe	EuGaSn
formula mass (g mol^{-1})	249.77	294.27	340.37
space group	*P*6/*mmm* (No.191)	$P6_3/mmc$ (No.194)	$P6_3/mmc$ (No.194)
lattice params (Å)	$a = 4.1687(6)$	$a = 4.2646(6)$	$a = 4.5243(5)$
	$c = 4.5543(9)$	$c = 18.041(5)$	$c = 18.067(3)$
vol (Å^3)	68.541(19)	284.15(9)	320.27(7)
Z	1	4	4
density calcd (g cm^{-3})	6.051	6.879	7.059
diffractometer	STOE IPDS	SMART Apex	SMART Apex
2θ range (deg)	4.48−69.64	4.48−55.94	5.0−55.88
index ranges	$-6 \le h \le 6$,	$-5 \le h \le 5$,	$-5 \le h \le 5$,
	$-6 \le k \le 6$,	$-5 \le k \le 5$,	$-5 \le k \le 5$,
	$-6 \le l \le 7$	$-23 \le l \le 23$	$-20 \le l \le 23$
reflns collected	1988	2203	1713
independent reflns	86 [$R_{init} = 0.076$]	169 [$R_{init} = 0.043$]	185 [$R_{init} = 0.030$]
data/refined params	86/7	169/12	185/11
GOF on F^2	1.185	1.259	1.297
final R indices [$I > 2\sigma(I)$]	R1 = 0.015,	R1 = 0.025,	R1 = 0.029,
	wR2 = 0.032	wR2 = 0.050	wR2 = 0.057
R indices (all data)	R1 = 0.015,	R1 = 0.032,	R1 = 0.036,
	wR2 = 0.032	wR2 = 0.053	wR2 = 0.059
largest diff. peak and hole (e$^-$/Å^3)	0.844/−0.705	0.800/−0.969	1.496/−2.123

Table 2. Atomic Coordinates and Equivalent Displacement Parameters for EuGaTt (Tt = Si, Ge, Sn)

atom	Wyckoff position	*x*	*y*	*z*	U_{eq}[a]
			EuGaSi		
Eu	1*a*	0	0	0	0.010(1)
Ga/Si	2*d*	1/3	2/3	1/2	0.017(1)
			EuGaGe		
Eu(1)	2*a*	0	0	0	0.010(1)
Eu(2)	2*b*	0	0	1/4	0.010(1)
Ga	4*f*	2/3	1/3	0.1467(1)	0.014(1)
Ge	4*f*	1/3	2/3	0.1142(1)	0.010(1)
			EuGaSn		
Eu(1)	2*a*	0	0	0	0.013(1)
Eu(2)	2*b*	0	0	1/4	0.010(1)
Ga	4*f*	2/3	1/3	0.1620(1)	0.014(1)
Sn	4*f*	1/3	2/3	0.1168(1)	0.011(1)

[a] U_{eq} is defined as one-third of the trace of the orthogonalized U_{ij} tensor.

Ga and Si atoms. The U_{33}/U_{11} ratio for the Ga/Si mixed site is large, which can indicate a tendency toward puckering the 6^3 anionic nets. To check the possibility of puckering, we refined the structure in space group $P\bar{3}m1$, which allowed the *z*-coordinate of the Ga/Si sites to refine: the result is $z = 0.5002(3)$. Therefore, we describe the unit cell of EuGaSi in the space group *P*6*mmm* where Ga and Si atoms are randomly distributed within the honeycomb net. Each Ga or Si atom is surrounded by three other main group atoms at the distance of 2.4068(3) Å. This distance is shorter than the sum of covalent radii of Ga and Si, which is 2.42 Å (r(Ga) = 1.25 Å, r(Si) = 1.17 Å[20]), implying significant interactions exist within the hexagonal layer.

EuGaGe and EuGaSn. EuGaGe and EuGaSn crystallize in the hexagonal YPtAs type of crystal structure which can be described as a puckered derivative of the AlB_2-type structure (see Figure 1).[35,36] The Ga and Ge/Sn atoms form puckered three-bonded, alternating hexagonal layers. Furthermore, the observed puckering mode locates Ga atoms closer (3.726(1) and 3.178(1) Å, respectively, for EuGaGe and EuGaSn) and Ge/Sn atoms farther to each other between adjacent layers. These Ga−Tt distances increase from EuGaGe to EuGaSn (see Table 3). Thus, as the Ga−Tt distance increases within the puckered sheets, the Ga−Ga distance between adjacent sheets decreases.

Since we observed a relatively high U_{33}/U_{11} ratio at the Ga site in EuGaGe, we attempted to refine a structure with a split Ga site. Although we were able to lower the *R* value from 2.45 to 2.40% with two additional parameters, a Hamilton significance test[37] suggested that the decrease of *R* value related to the additional parameters was not a significant improvement. Therefore, in the absence of any other reason to split the Ga site, we will use the originally refined structure.

The indistinguishable atomic positions for Ga and Ge in EuGaGe can be differentiated for Ga and Sn in EuGaSn and agree with total energies obtained from electronic structure calculations. However, we could distinguish Ga and Ge atomic positions based on the differential isotropic thermal

Table 3. Selected Interatomic Distances and Bond and Torsion Angles for EuGaTt (Tt = Si, Ge, Sn)

	EuGaSi		EuGaGe	EuGaSn
Ga−Tt (Å)	2.4068(3)		2.5312(7)	2.7369(7)
Ga−Ga (Å)	4.5543(9)		3.726(1)	3.178(1)
Eu−Ga/Si (Å)	3.3133(4)	Eu(1)−Ga (Å)	3.615(1)	3.924(1)
		Eu(1)−Tt (Å)	3.210(1)	3.3585(7)
		Eu(2)−Ga (Å)	3.088(1)	3.057(1)
		Eu(2)−Tt (Å)	3.474(1)	3.5512(8)
Ga−Tt−Ga (deg)	120.0		114.79(4)	111.49(4)
torsion angle (Ga−Tt−Ga−Tt, deg)	0		43.8	54.7

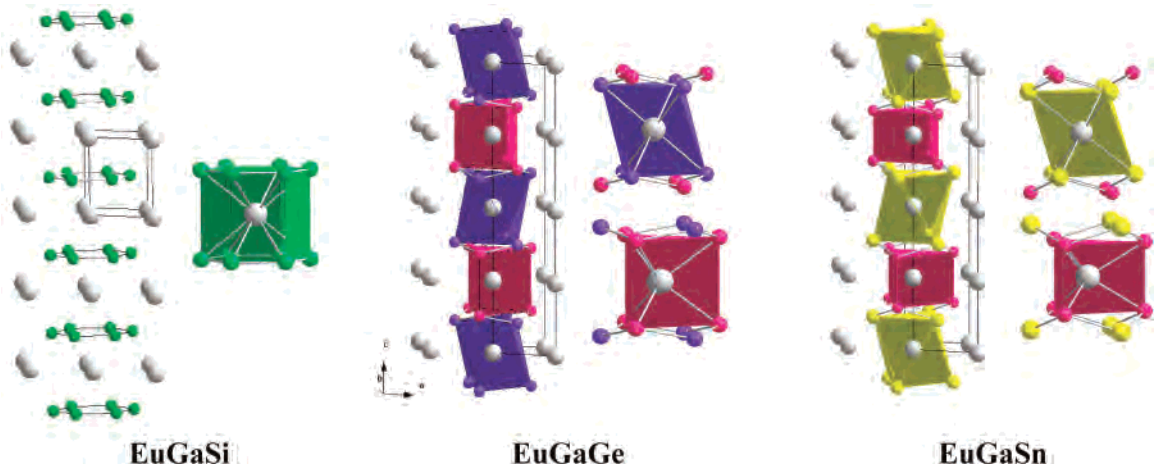

Figure 1. Crystal structures of EuGaSi, EuGaGe, and EuGaSn and coordination environments at the Eu atoms: Eu, gray; Ga/Si, green; Ga, red; Ge, purple; Sn, yellow.

displacement parameters, U_{11}, at two 4f sites. Refinements of structures with either *only* Ge atoms or *only* Ga atoms at the two 4f sites in the asymmetric unit produced smaller U_{11} values at the Ga site than at the Ge site by 25 and 33%, respectively, suggesting lower electron accumulation at the Ga site. However, we observed equal U_{11} values at the two 4f sites when we differentiated the Ga and Ge atomic positions as shown in Supporting Information (Table S2).

There are two distinct coordination environments at the Eu sites, as also shown in Figure 1: Eu(1) is surrounded by an octahedron of six Ge or Sn atoms, whereas Eu(2) is surrounded by six Ga atoms forming a trigonal prism. As listed in Table 3, the nearest neighbor distances of these two Eu coordination polyhedra change in opposing fashion: Eu−Ge/Sn distances for the octahedra increase, while Eu−Ga distances in the trigonal prisms decrease from EuGaGe to EuGaSn.

Along the entire EuGaTt series, as the size of the Tt atom increases, the torsion angle of the polyanion layer increases, indicating the change from planar to moderately puckered and then strongly puckered layers. The torsion angles of the puckered hexagonal layers in EuGaGe and EuGaSn can be compared with several known analogues, such as CaGaGe and SrGaSn.[38] These compounds show increasing torsion angles from 42.20 (CaGaGe) and 43.80 (EuGaGe) to 54.70 (EuGaSn) and 56.07° (SrGaSn) as the size of active metal or Tt atom increases (ionic radii $r(Ca^{2+}) = 1.06$ Å, $r(Eu^{2+}) = 1.12$ Å, $r(Sr^{2+}) = 1.27$ Å; covalent radii $r(Ge) = 1.22$ Å, $r(Sn) = 1.40$ Å).[20] In addition, on going from EuGaSi to EuGaGe and EuGaSn, the lattice parameter a increases, whereas the average separation between $^2_\infty$[GaTt] sheets, as measured either by c for EuGaSi or $c/4$ for EuGaGe and EuGaSn, decreases. The interlayer Ga−Ga distance between adjacent hexagonal layers significantly decreases as the size of Tt atom increases.

For comparison, the gallium monochalcogenides, GaS,[39] GaSe,[40] and HT-GaTe,[41] represent a series isoelectronic with EuGaTt (HT-GaTe is reported as the "high-temperature" form; at ambient conditions, the crystal structure of GaTe is monoclinic).[42] These binary compounds adopt structures closely related to the [GaGe] and [GaSn] networks in EuGaGe and EuGaSn but not to the [GaSi] framework in EuGaSi. In GaX (X = S, Se, Te), however, the $^2_\infty$[GaX] sheets are significantly more puckered as evidenced by the Ga−X−Ga angles (all ∼100°) and their corresponding torsion angles (all ∼76°). As the size of X increases, the Ga−X distances increase from 2.332 (GaS) to 2.453 (GaSe) and to 2.612 Å (GaTe), whereas the Ga−Ga separation varies as 2.449 (GaS), 2.444 (GaSe), and 2.714 Å (GaTe). Therefore, the Ga−Tt distances in EuGaTt fall in a similar range to the Ga−X contacts in GaX, but the corresponding Ga−Ga distances are much longer in the EuGaTt series. We will explore the chemical bonding issues in EuGaTt in a subsequent section of this paper.

Magnetic Susceptibilities. Temperature-dependent magnetic susceptibilities and reciprocal susceptibilities of all three compounds are measured at 0.1 T and shown in Figure 2. The susceptibility curves show essentially Curie−Weiss behavior in the corresponding paramagnetic regions with ferromagnetic (FM) behavior for EuGaSi and EuGaGe and antiferromagnetic (AFM) behavior for EuGaSn at low temperatures. Magnetization measurements as a function of external field (0−5.5 T) at 2 K confirmed these magnetic ordering characteristics for each compound. Fitting of the linear $1/\chi$ versus T curves above ∼120 K gives the effective magnetic moments to be 7.93(1) μ_B for EuGaSi, 7.97(1) μ_B for EuGaGe, and 7.99(1) μ_B for EuGaSn, moments which are all very close to the value of the Eu^{2+} free ion, 7.94 μ_B, to indicate a $4f^7$ electronic configuration for Eu. Small

(35) Hoffmann, R.; Pöttgen, R. *Z. Kristallogr.* **2001**, *216*, 127.
(36) Burdett, J. K.; Miller, G. J. *Chem. Mater.* **1990**, *2*, 12−26.
(37) Hamilton, C. W. *Acta Crystallogr.* **1965**, *18*, 502−510.
(38) Czybulka, A.; Pinger, B.; Schuster, H. *Z. Anorg. Allg. Chem.* **1989**, *579*, 151−157.
(39) Kuhn, A.; Bourdon, A.; Rigoult, J.; Rimsky, A. *Phys. Rev. B* **1982**, *25*, 4081−4088.
(40) Benazeth, S.; Dung, N. H.; Guittard, M.; Laruelle, P. *Acta Crystallogr., Sect. C* **1988**, *44*, 234−236.
(41) Semiletov, S. A.; Vlasov, V. A. *Kristallografiya* **1963**, *8*, 877−883.
(42) Julien-Pouzol, M.; Jaulmes, S.; Guittard, M.; Alapini, F. *Acta Crystallogr., Sect. B* **1979**, *35*, 2848−2851.

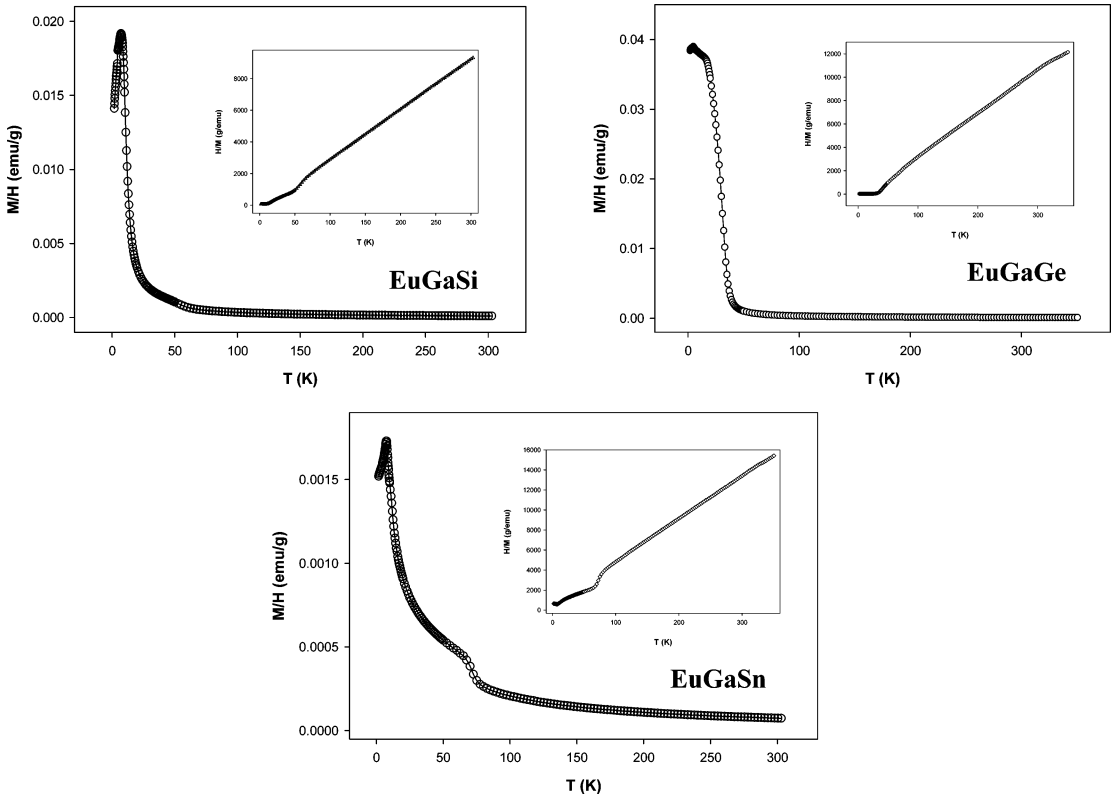

Figure 2. Temperature dependence of the magnetic susceptibilities and the reciprocal susceptibilities for EuGaSi, EuGaGe, and EuGaSn.

shoulders observed in the $\chi(T)$ curves for EuGaSi and EuGaSn arise from trace amounts of EuO, which is reported to show FM ordering at ~70 K.[43−45] This impurity can also be observed in the powder X-ray diffraction pattern of EuGaSn, but it is not noticeable in the pattern of EuGaSi. Since a small amount of EuO exists in products (according to powder X-ray pattern), it cannot significantly affect the results of magnetic susceptibility measurements of major phases.

Both EuGaSi and EuGaGe show Curie−Weiss behavior, respectively, at temperatures above 86(5) K and 95(5) K. Below those temperatures, the susceptibilities become dependent on the external magnetic field and show FM ordering with $\theta_p = +8.8(5)$ K for EuGaSi and $\theta_p = +14.5(5)$ K for EuGaGe. EuGaSn is Curie−Weiss paramagnetic above 116-(5) K but shows AFM ordering with $\theta_p = -15.2(5)$ K.

Eu L_{III} XAS Measurements. As shown in Figure 3, sharp absorption maxima are observed at ~6977 eV for all three EuGaTt (Tt = Si, Ge, Sn) samples, which indicates a $4f^7$ electronic configuration at the Eu atoms for the entire series. These results are consistent with the magnetic susceptibility data. Small shoulders observed at approximately 10 eV higher than the main absorption peak are the result of the existence of small traces of another form of Eu impurity, Eu_2O_3 (electronic configuration $4f^6$, Eu^{3+}) in all three samples.

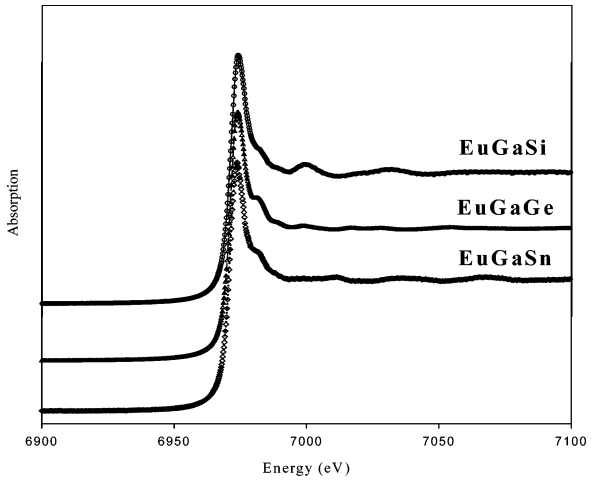

Figure 3. XAS spectra of EuGaTt (Tt = Si,Ge,Sn).

Electronic Structure Calculations. To investigate the electronic structure and chemical bonding features that contribute to the structural trends and atomic distributions in EuGaTt, TB-LMTO-ASA electronic structure calculations using spin-polarized LSDA were carried out on observed crystal structures, as well as on several hypothetical structural models. For these systems, the DOS curves for the majority and minority spin states differed only slightly, so subsequent DOS curves illustrate their superpositions.

EuGaSi. X-ray diffraction results showed a complete absence of ordering of Ga and Si in this AlB_2-type structure. Therefore, we constructed three ordered, model structures for EuGaSi, which are illustrated in Figure 4. In all three models, we fixed every $^2_\infty$[GaSi] layer to be ordered with

(43) Pöttgen, R.; Johrendt, D. *Chem. Mater*. **2000**, *12*, 875−897.
(44) McWhan, D.; Souers, P.; Jura. G. *Phys. Rev*. **1966**, *143*, 385−389.
(45) Stroka, B.; Wosnitza, J.; Scheer, E.; Löhneysen, H.; Park, W.; Fischer, K. *Z. Phys. Condens. Matter*. **1992**, *89*, 32.

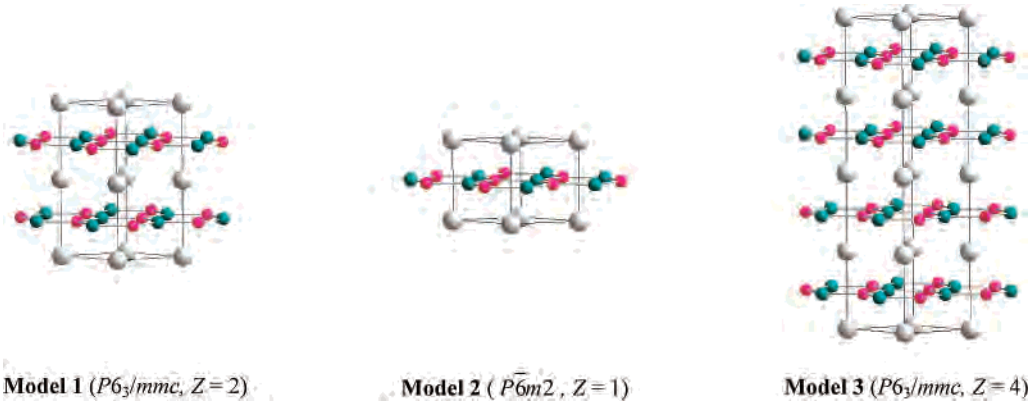

Figure 4. Three structural models of EuGaSi: Eu, gray; Ga, red; Si, green. See text for detailed descriptions.

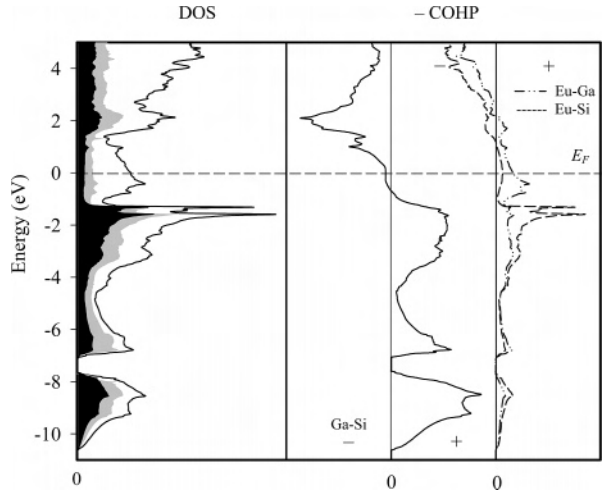

Figure 5. DOS and COHP curves for EuGaSi. (Left) Total DOS (solid line), Eu PDOS (white region), Ga PDOS (gray region), and Si PDOS (black region). (Right) Ga−Si, Eu−Ga, and Eu−Si COHP curves. The Fermi level is indicated by the dashed line and is the energetic reference (0 eV).

only Ga−Si contacts (an alternant 6^3 net). For the isoelectronic system, MAlSi (M = Ca, Sr), Mazin and Papaconstantopoulos investigated the influence of in-plane ordering using the virtual crystal approximation to average Al and Si. They concluded that in-plane Al−Si ordering did not affect the band structures or DOS curves of these systems significantly.[46]

Our three models differ from each other in how these alternate 6^3 sheets stack along the *c*-axis: (1) alternating to create just Ga···Si interactions between planes, space group $P6_3/mmc$, $Z = 2$; (2) eclipsed to create Ga···Ga and Si···Si interactions between planes, space group $P\bar{6}m2$, $Z = 1$; and (3) 1:1 intergrowth of models 1 and 2 to create Ga···Si, Ga···Ga, and Si···Si interactions between planes, space group $P6_3/mmc$, $Z = 4$. Model 3 has a unit cell that resembles most closely the structures of EuGaGe and EuGaSn. The calculated total energies give model 1 as slightly more energetically favorable than both model 2, by just 0.75 meV/formula unit (fu), and model 3, by 0.14 meV/fu

Figure 5 illustrates DOS and COHP curves for Model 1, where the Fermi level (E_F) is the reference energy value in these curves. Throughout the entire DOS curve, there is significant mixing between valence orbitals of Eu and Ga/Si atoms. The region below approximately −1.0 eV displays significant contributions from Ga and Si atoms, whereas the region above approximately −1.0 eV is dominated by valence orbitals at Eu. In the occupied region of the DOS curve, there are three principal segments: (a) a bonding valence 3s−4s band between ∼8.0 and 10.5 eV below E_F, (b) a bonding 3p−4p band between ∼1.0 and 7.0 eV below E_F, and (c) a Eu 5d band around E_F. A deep minimum (almost a "pseudogap") in the DOS curve at ∼1.0 eV below E_F corresponds to a valence band filling of 8 valence electrons per formula unit, which nearly matches the top of the Ga−Si bonding states shown in the adjacent COHP curve. In fact, the Fermi level for EuGaSi falls in the Ga−Si nonbonding region, whereas the Eu−Ga and Eu−Si COHP curves indicate bonding states at the Fermi level. Integration of the DOS curve and the electronic band structure (available in Supporting Information) reveals that Ga−Si σ-bonding bands span the region between ∼1.0 and 7.0 eV below E_F (segment b above), and Ga−Si π-bonding bands start ∼5 eV below E_F. Orbital interactions between $^2_\infty$[GaSi] planes along the *c*-axis take place primarily via the intervening Eu atoms, such that a Eu 5d band drops below E_F. Therefore, Ga−Si orbital interactions are predominantly two-dimensional in character.[47]

The strong doubled peak in the DOS has two origins: (1) from a nearly flat band composed of valence p_x and p_y orbitals from Ga and Si along the ΓM line in the first Brillouin zone, a band that remains relatively flat up to the AL line at the zone boundary, and (2) a nearly dispersionless band valence p_z orbitals from Ga and Si along the ΓK line. This second band shows nearly zero dispersion through changing overlap with Eu 5d orbitals along the ΓK direction. A "fatband" analysis[21,28] of the electronic band structure for EuGaSi is available in Supporting Information. These peaks are a distinct feature of the DOS curves for AlB_2-type structures with large "cations", for example, BaAlSi.[48] A study of the electronic structures of AEAlSi (AE = Ca, Sr, Ba)[44] showed a distinct change in the corresponding DOS curves as the size of AE changed. In BaAlSi, an energy gap

(46) Mazin, I. I.; Papaconstantopoulos, D. A. *Phys. Rev. B* **2003**, *68*, 220504(R).
(47) Giantomassi, M.; Boeri, L.; Bachelet, G. *Phys. Rev. B* **2005**, *72*, 224512.
(48) Huang, G. Q.; Chen, L. F.; Liu, M.; Xing, D. Y. *Phys. Rev. B* **2004**, *69*, 064509.

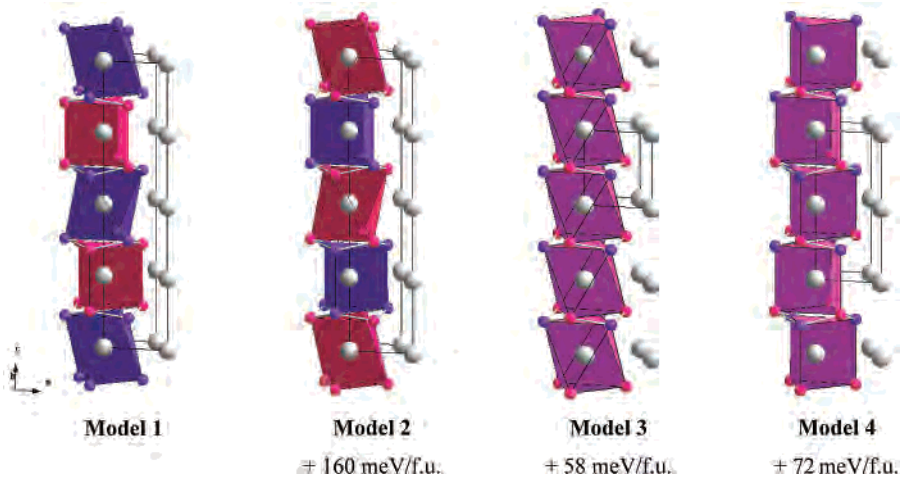

Figure 6. Four structural models of EuGaGe: Eu, gray; Ga, red; Ge, purple. See text for detailed descriptions.

opened for 8 valence electrons, with a sharp double peak in the DOS just below this gap. The DOS curves for SrAlSi and CaAlSi showed no energy gap and a much reduced peak. Reasons for the differences in AEAlSi include (a) decreasing bandwidths for the occupied valence bands as the AE size increases because of smaller Al−Si orbital overlaps and (b) increased orbital mixing between the valence p_z orbitals of the Al−Si network and the valence d orbitals of the AE atoms. We continue to investigate how such subtle interactions can impact structural features and physical properties in these and related polar intermetallic systems.

EuGaGe and EuGaSn. Both EuGaGe and EuGaSn, which are isoelectronic to EuGaSi, crystallize in the YPtAs-type structure instead of the AlB_2-type structure. The $^2_\infty$[GaTt] sheets are no longer planar, and interlayer Ga···Ga contacts at 3.726(1) and 3.178(1) Å in EuGaGe and EuGaSn, respectively, suggest an attractive, albeit weak, interaction at least for EuGaSn. To explore these distinct features, as well as to identify the most favorable atomic distributions, the total energies of four structural models of EuGaTt shown in Figure 6 have been calculated by TB-LMTO-ASA calculations. In this section, we report computational results for EuGaGe because we were particularly interested in assessing the Ga/Ge distributions. EuGaSn and EuGaGe show very similar electronic band structures, provided in Supporting Information.

Models 1 and 2 are the observed geometrical structures; both differ in how Ga and Ge atoms are arranged: model 1 is the "observed" arrangement with closer Ga···Ga contacts between $^2_\infty$[GaGe] sheets, and model 2 is the alternative structure, with shorter Ge···Ge contacts. The other two models explore the coordination at Eu: model 3 contains only octahedrally coordinated Eu sites, as in the $EuGe_2$-type structure, whereas model 4 contains only trigonal prismatic coordinated Eu sites. The total energies revealed that model 1 is the most favorable structure. The energy difference of 160 meV/fu between models 1 and 2 suggests a strong electronic influence for the observed "coloring" scheme. Models 3 and 4 give intermediate energy values, which again point to electronic factors dictating the geometrical preferences in this system.

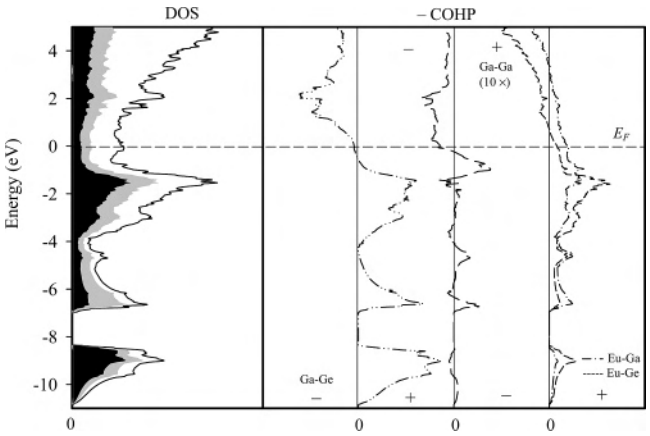

Figure 7. DOS and COHP curves for EuGaGe. (Left) Total DOS (solid line), Eu PDOS (white region), Ge PDOS (black region), and Ga PDOS (gray region). (Right) Ga−Ge, Ga−Ga, Eu−Ga, and Eu−Ge COHP curves. Ga−Ga COHP curve is magnified by ten times for comparison. The Fermi level is indicated by the dashed line and is the energetic reference (0 eV).

The DOS and Ga−Ge, Ga−Ga, Eu−Ga, and Eu−Ge COHP curves for EuGaGe in model 1 are illustrated in Figure 7. These curves are qualitatively similar to those for EuGaSi except for two features: (a) the sharp valence p_x and p_y peak ~1.7 below E_F is less pronounced in EuGaGe than in EuGaSi, and (b) the Eu 5d band eliminates the deep minimum clearly visible in the DOS for EuGaSi. These characteristics reflect the different electronic character between Si and Ge as well as different structures. Although these subtle differences exist in the DOS curves, the corresponding COHP curves are quite similar to those for EuGaSi: the Ga−Ge and Eu−Ge contacts are nearly optimized in both.

To understand the origin of the energy difference between models 1 and 2, the corresponding ICOHP values are listed in Table 4 to compare the various orbital interactions within each model. According to these results, Ga−Ge, Eu−Ge, and Eu−Ga interactions are attractive in both models, whereas the Ga−Ga interaction between $^2_\infty$[GaGe] sheets, only, in model 1 is (weakly) attractive. The Ga−Ga COHP curve (see Figure 7) crosses from bonding to antibonding states at the Fermi level. These interactions lead to the

Table 4. Integrated Crystal Orbital Hamiltonian Population (ICOHP) Values Per Bond for Models 1 and 2 of EuGaGe[a]

model 1			model 2		
bond	distance (Å)	ICOHP	bond	distance (Å)	ICOHP
Ga−Ge	2.5314(7)	−0.2007	Ga−Ge	2.5314(7)	−0.2022
Ga−Ga	3.726(1)	−0.0109	Ga−Ga	4.800(1)	+0.0024
Ge−Ge	4.800(1)	+0.0043	Ge−Ge	3.726(1)	+0.0034
Eu(2)−Ga	3.087(1)	−0.0560	Eu(1)−Ga	3.087(1)	−0.0590
Eu(1)−Ge	3.210(1)	−0.0645	Eu(2)−Ge	3.210(1)	−0.0626

[a] Negative and Positive ICOHP Values Represent, Respectively, Net Bonding and Antibonding Interactions.

different coordination environments at the Eu sites and the observed puckering of the $^2_\infty$[GaGe] sheets.

Chemical Bonding Analysis. Polar intermetallic compounds, like the EuGaTt examples reported in this work, often adopt structures in agreement with the Zintl−Klemm concept.[4,8] The success of this electron-counting rule is high when the compounds show semiconducting (nonmetallic) behavior, but it frequently requires modification or explanation when the compounds are metallic, such is the anticipated case for EuGaTt. Magnetic and spectroscopic measurements confirm the $4f^7$ configuration at the Eu sites, so we can formulate the main group component as $[GaTt]^{2-}$, which is assigned 9 valence electrons. According to the Zintl−Klemm concept,[8] the three-connected 6^3 nets would then be formulated as $[(3b)Ga^{2-}(3b)Tt^{-}] = [GaTt]^{3-}$, which is optimized for 10 valence electrons. For *planar* 6^3 nets, as in graphite, the formulation $[(4b')Ga^{-}(4b')Tt^{0}] = [GaTt]^{-}$ becomes more realistic as π-interactions become influential and is optimized for 8 valence electrons. Clearly, the EuGaTt series is an intermediate case.

The DOS curves for EuGaTt all show minima in the DOS at 8 valence electrons and is deepest for EuGaSi, which partially substantiates the simple electron-counting rule. EuGaSi differs from EuGaGe and EuGaSn in how the additional valence electron is used for chemical bonding: puckering of the 9-electron $[GaGe]^{2-}$ and $[GaSn]^{2-}$ sheets to give Ga···Ga contacts implies the formulations $[(4b)Ga^{-}(3b)Ge^{-}]$ and $[(4b)Ga^{-}(3b)Sn^{-}]$.

However, these Ga···Ga contacts exceed 3.0 Å, which is not consistent with 2-center, 2-electron bonding between these Ga atoms. No such distortion occurs in EuGaSi, which resembles the situation in 9-electron AlB_2. The isoelectronic gallium monochalcogenides, GaX (X = S, Se, Te), follow the Zintl−Klemm formalism more closely than EuGaTt: the Ga−Ga distances are less than 2.75 Å, so the formulation would be $[(4b)Ga^{-}(3b)X^{+}]$. However, the formal charges assigned to each site violate expectations from electronegativity arguments. The limiting ionic formulation is $Ga^{2+}X^{2-}$. Since there are no Tt−Tt contacts in EuGaTt, we may consider the formulation $Eu^{2+}Ga^{2+}Tt^{4-}$, but this is certainly an extreme and highly unrealistic picture of the bonding situation.[8]

Extended Hückel (EHT) calculations[49,50] on two model structures derived from EuGaGe can provide some preliminary insights into the factors influencing how these layers shift away from planar configurations. These model structures consist of two planar, alternate $^2_\infty$[GaGe]$^{2-}$ 6^3 nets stacked in an eclipsed fashion to give interplanar Ga···Ga and Ge···Ge contacts (see Figure 8); the two cases differ by whether or not there are Eu atoms inserted between these planes. For the calculations, the interplanar distance was kept fixed at 4.00 Å, while the *a*-axis was varied. Trends in crystal orbital overlap population (COOP) values for Ga−Ge, Ga···Ga, and Ge···Ge contacts are plotted as a function of lattice constant. When no Eu atoms occur between these planes, the results show that as the Ga−Ge distance increases, the corresponding interplanar Ga···Ga overlap population is significantly bonding and also increases, while the Ge···Ge overlap population remains nearly zero, that is, essentially nonbonding. With inserted Eu atoms, the Ga···Ga overlap populations drop to nonbonding values. In this case, both Ga···Ga and Ge···Ge contacts are weakly repulsive, with the stronger orbital repulsions occurring within the Ge···Ge contacts. Thus, this semiempirical analysis suggests that the puckering is influenced by Eu−Ga and Eu−Ge interactions rather than through-space Ga···Ga interactions.

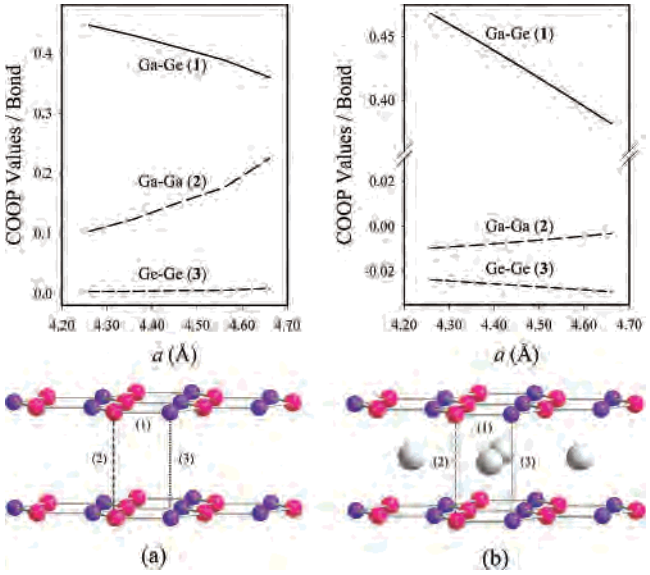

Figure 8. (a) Model structure $^2_\infty[(GaGe)_2]^{4-}$ and (b) model structure $^2_\infty[Eu(GaGe)_2]^{4-}$ with corresponding COOP analysis of Ga−Ge, Ga···Ga, and Ge···Ge contacts as the unit cell parameter *a* varies.

Bonding Analysis by the Electron Localization Function (ELF). Because the formation of an electron pair is the key element of the models for the chemical bond, it becomes possible to describe chemical bonding using so-called bonding-detector functions, for example, the electron localization function (ELF)[27a] or the electron localizability indicator (ELI),[27b] both of which are related to the motion of

(49) (a) Hoffmann, R. *J. Chem. Phys.* **1963**, *39*, 1397. (b) Hoffmann, R.; Lipscomb, W. N. *J. Chem. Phys.* **1962**, *36*, 2179. (c) Whangbo, M.-H.; Hoffmann, R.; Woodward, R. B. *Proc. R. Soc. London* **1979**, *A366*, 23.

(50) EHT calculations included orbital overlaps within second-nearest neighbor unit cell with Hamiltonian matrix elements calculated by the weighted Wolfsberg−Helmholz expression.[51] Integrated COOP values were evaluated by 200 *k*-points in the first Brillouin zone. Atomic orbital parameters are as follows: Ga 4s, $H_{ii} = -14.58$ eV, $\zeta = 1.77$; Ga 4p, $H_{ii} = -6.75$ eV, $\zeta = 1.55$; Ge 4s, $H_{ii} = -16.00$ eV, $\zeta = 2.16$; Ge 4p, $H_{ii} = -9.00$ eV, $\zeta = 1.85$; Eu 6s, $H_{ii} = -8.13$ eV, $\zeta = 1.74$, Eu 6p, $H_{ii} = -5.13$ eV, $\zeta = 1.70$, Eu 5d, $H_{ii} = -8.32$ eV, $\zeta_1 = 1.56$ (0.8316), $\zeta_2 = 3.55$ (0.3041).

(51) Ammeter, J. H.; Bürgi, H.-B.; Thibeault, J. C.; Hoffman, R. *J. Am. Chem. Soc.* **1978**, *100*, 3686.

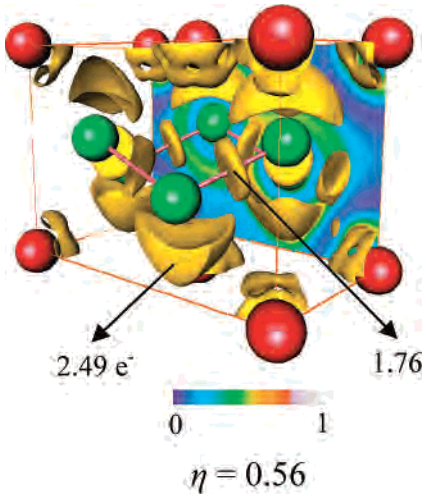

Figure 9. ELF distribution (color scale indicated) in $EuGe_2$: Eu sites, red spheres; Ge sites, green spheres. ELF isosurfaces ($\eta = 0.56$), colored in yellow, produce lone-pair attractors (2.49 e^-) and Ge−Ge bond pair attractors (1.76 e^-). A (110) ELF surface is also illustrated.

electron pairs in a chemical system. In this bonding analysis of EuGaTt, we use the system of tools based on ELF. In the ELF representation, the elements of chemical bonding are consequently derived by employing the topological features of the bonding-detector function. The directed interaction between atoms in a chemical structure, that is, a molecule or extended solid, can be distinguished in real space. Maxima of the ELF in the valence region (valence shells) or structurization of the penultimate (outer core) shell[27c] provide signatures for directed (covalent) bonding. The ELF tools are especially suitable to detect directed (covalent) bonding in materials with bands that are not fully occupied or are strongly overlapping, a situation which is typical for intermetallic compounds. The analysis of the topology of ELF can be combined with the consecutive integration of the electron density in "basins," which are bound by zero-flux surfaces in the ELF gradient field. This procedure, similar to the one proposed for electron density,[30] allows assignment of an electron count for each basin, revealing basic information about chemical bonding. This combined application of ELF together with electron density offers the possibility of Zintl-like electron counts for a large group of intermetallic phases and of getting access to a bond definition in real space for complex structures. Reviews on the application of ELF for different kinds of bonding situations are available;[27d] for more details, see http://www.cpfs.mpg.de/ELF.

ELF can be illustrated in two distinct ways: (1) as surfaces corresponding to a single ELF value ("isosurfaces") and (2) as a slice through the structure. To achieve further insights into the valence region along the EuGaTt series, especially between Ga atoms, the ELF has been analyzed in detail for EuGaSi and EuGaSn (EuGaSn was selected because the interlayer Ga···Ga contact is significantly shorter than the corresponding distance in EuGaGe). To have a reference system with puckered main group 6^3 nets for comparison, an ELF analysis on $EuGe_2$ was also conducted.

$EuGe_2$. The topological analysis of ELF reveals four attractors, which are defined as local maxima of ELF values, around each three-bonded Ge atom as shown in Figure 9. One lone-pair-like attractor is located above (or below) the atom along [001], and three other attractors are symmetrically located at Ge−Ge contacts within the hexagonal layer. Integration of the total electron density within each basin, which is defined by zero-flux surfaces in the ELF gradient, gives the valence electron counts of 2.49 electrons for the lone-pair-like attractor and 1.76 electrons for the Ge−Ge bond attractors. Thus, the total valence electron count for valence shell basin sets is 5.13 electrons per Ge atom (2.49 e^- ("lone pair") + 3 × 1.76 $e^-/2$ ("bond pairs")), which can be written as $Ge^{1.13-}$. As a result, the bonding situation in $EuGe_2$ may be described as $Eu^{2.26+}[Ge^{1.13-}]_2$, which agrees reasonably well with a Zintl−Klemm representation as $Eu^{2+}[Ge^-]_2$.

EuGaSi. (Figure 10) ELF attractors are located around the three-bonded Ga and Si atoms within the planar polyanionic layers. Unlike $EuGe_2$, lone-pair-like attractors are observed symmetrically above and below both Ga and Si atoms along [001], together with bond attractors on each Ga−Si bond. Integration of the total electron density of lone-pair-like attractors around Ga and Si atom and the Ga−Si bond attractors results in values of 3.81 electrons for the valence shell basins of Ga and 5.32 electrons for the valence shell basins of Si for a formulation of $Eu^{2.13+}[Ga^{0.81-}Si^{1.32-}]$ with roughly divalent Eu atoms.

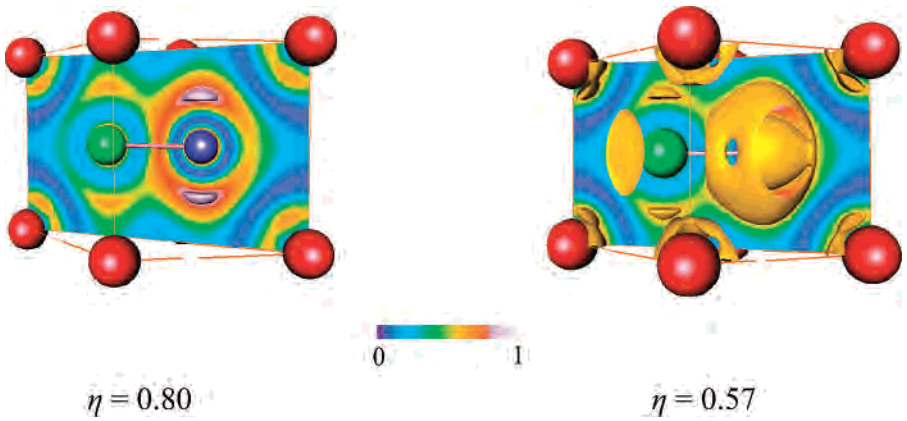

Figure 10. ELF distribution (color scale indicated) in EuGaSi: Eu sites, red spheres; Ga sites, green spheres; Si sites, blue spheres. ELF isosurfaces ($\eta =$ 0.80 and 0.57), colored, respectively, in white and yellow, produce attractors associated with Si and Ga atoms. A (110) ELF surface is also illustrated.

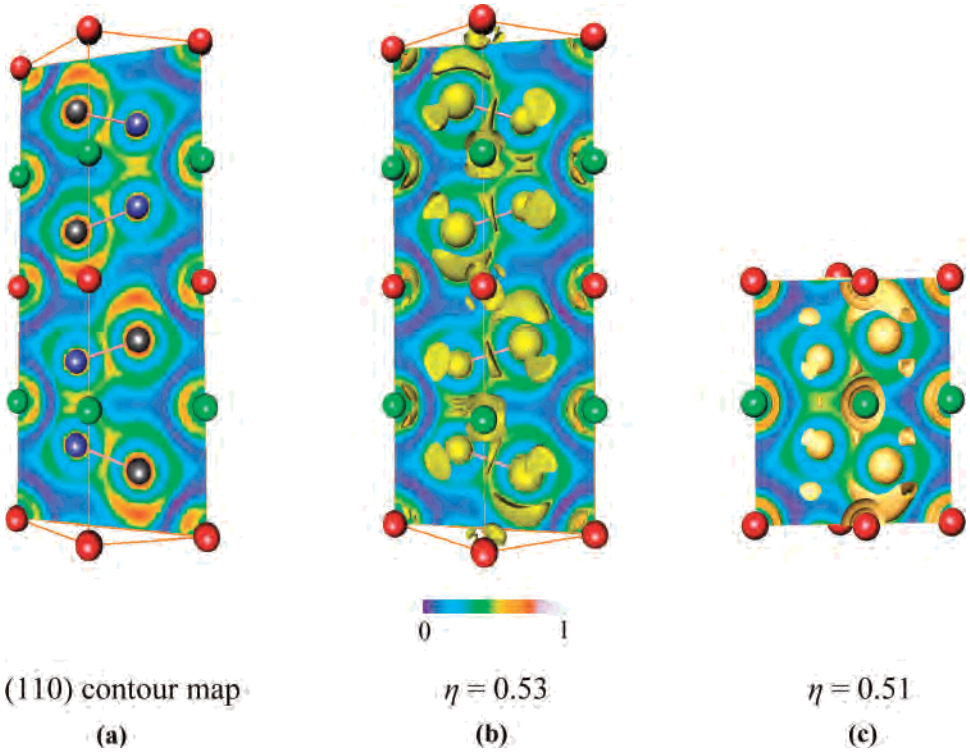

Figure 11. (a) ELF distribution of EuGaSn (LMTO calculations) in the (110) plane. (b) ELF isosurface ($\eta = 0.53$) interspersed with (110) ELF distribution. (c) One-half of a unit cell of EuGaSn with ELF isosurface ($\eta = 0.51$) based on a FPLO calculation: Eu(1) sites, red spheres; Eu(2) sites, green spheres; Ga sites, blue spheres; Sn sites, black spheres.

EuGaSn. (Figure 11) The positions of ELF bond attractors around three-bonded Ga and Sn atoms are similar to those in $EuGe_2$ and EuGaSi. Since the extent of puckering for each $^2_\infty$[GaSn] layer is between that of $EuGe_2$ and EuGaSi, we observe lone-pair-like attractors on Ga and Sn atoms along [001]. The lone-pair-like attractors at each Ga site face each other as shown in Figure 11b and show two maxima within this pair. Clearly, the Ga···Ga contact does not show a bond attractor as seen for the Ga−Sn contacts. Integration of the total valence electron density in the basins was performed as described earlier for $EuGe_2$ and EuGaSi and formulated EuGaSn to be $Eu^{2.12+}[Ga^{0.54-}Sn^{1.58-}]$.

This type of interaction is also observed in a full-potential local orbital calculation (FPLO), which confirms the existence of two separate attractors between Ga atoms as shown in Figure 11c. Therefore, this interaction cannot be identified as a two-center, two-electron bond. Rather, we suggest these interlayer Ga···Ga interactions to be described as two distinct four-center interactions involving one Ga atom and three Eu atoms forming a distorted tetrahedral surrounding of this attractor. This is well in agreement with the population analysis from both TB-LMTO-ASA and EHT revealing a pronounced Eu−Ga and Eu−Ge interaction and an essentially nonbonding Ga−Ga interaction. We continue to explore this unusual interaction with theoretical calculations and high-pressure experiments on EuGaTt.

Summary

Three ternary compounds EuGaTt (Tt = Si, Ge, Sn) were prepared, and their crystal structures were characterized by powder and single-crystal X-ray diffraction. EuGaSi crystallizes in the AlB_2-type structure with a planar hexagonal layer consisting of randomly distributed Ga and Si atoms, whereas EuGaGe and EuGaSn adopt the YPtAs-type of crystal structure with puckered polyanionic layers composed of ordered Ga and Ge/Sn atoms. On the basis of the crystal structure refinement, two distinct coordination environments at Eu, octahedral and trigonal prismatic, were found in EuGaGe and EuGaSn. Electronic factors are influential to direct the distribution of Ga and Tt atoms in these structures, which also affect local structural distortions. An unusual four-center interaction is revealed by ELF calculations.

Acknowledgment. This work was supported by NSF DMR 02-41092 and 06-05949. The authors are grateful to Dr. Warren Straszheim for the EDXS measurements, to Dr. Sergey Bud'ko for magnetization measurements at Iowa State University, to Dr. Ulrich Burkhardt for XAS measurements, to Dr. Alexei Baranov for FPLO calculations, as well as to Dr. Frank Wagner and Dr. Miroslav Kohout at Max-Planck-Institute for Chemical Physics of Solids in Dresden, Germany, for a fruitful discussion concerning bonding analysis in real space. T.-S.Y. also wishes to thank MPI-CPFS in Dresden, Germany, for financial support.

Supporting Information Available: X-ray crystallographic files in CIF format, results from alternative synthetic procedures, lattice constants as determined by single-crystal and powder X-ray diffraction, anisotropic displacement parameters, field-dependent magnetization curves, and electronic band structures for EuGaTt (Tt = Si, Ge, Sn). This material is available free of charge via the Internet at http://pubs.acs.org.

IC701111E